Simulation and Design of Monolithically Integrated Tunable Wavelength Converter Based on V-cavity Laser and Delayed Mach-Zehnder Interferometer

Yingchen Wu and Jian-Jun He
State Key Laboratory of Modern Optical Instrumentation, Centre for Integrated Optoelectronics
Department of Optical Engineering, Zhejiang University, Hangzhou 310027, China

Abstract— In this paper, we present the design and simulation results of a much simpler monolithically integrated wavelength converter based on a V-cavity laser (VCL) and delayed Mach-Zehnder interferometer (DMZI) with semiconductor optical amplifiers (SOAs). The dynamic characteristics of the wavelength converter are investigated using the large-signal dynamic model of semiconductor optical amplifier (SOA) with time-dependent transfer matrix method (TD-TMM). A 10 Gb/s return-to-zero (RZ) tunable all-optical wavelength converter is achieved with a large extinction ratio for both frequency up and down conversions.

1. INTRODUCTION

The rapid growth of internet and internet-related services calls for large-capacity and high-speed data networking. Optical networking allows for data reconfiguration directly in the optical layer rather than electrical layer. Since little electronic processing involved, the electronic bottle-neck can be avoided. The key to making optical packet routing (OPR) practical and cost-effective is in realizing the full potential of photonic integrated circuits. OPR technologies hold promise to provide the largest granularity with more efficient power and footprint scaling [1].

A variety of optical routing technologies have been proposed for use in OPR, which can be divided into two categories: space-switch-only [2–4] and wavelength-reconfigurable-routing [5, 6]. The later technique is more promising due to its flexibility and high scalability for larger throughput. However, it usually involves multi-epitaxial regrowth and some other complicated fabrication techniques. Tunable wavelength converters are very useful for realizing reconfigurable wavelength routers.

The focus of this paper is the simulation and design of a 10 Gb/s return-to-zero (RZ) tunable all-optical wavelength converter for use in OPR. The device is based on monolithically integration of a V-cavity laser and delayed Mach-Zehnder interferometer (DMZI) with semiconductor optical amplifiers (SOAs). Only one epitaxial regrowth is needed to realize the offset quantum-well integration platform, and no grating structure is required in the design, which leads to a much simpler device processing routine.

2. DEVICE INTEGRATION ARCHITECTURE

The device requires a single-input a single-output fiber. Figure 1 is the schematic of the wavelength converter. The device consists of a widely-tunable V-cavity laser (VCL), a delay waveguide, a differential MZI-SOA wavelength converter, and pre-amplifies SOAs. The on-chip VCL, which consists of two Fabry-Perot cavities coupled through a half-wave coupler, offers simple and efficient wavelength switching with 100 GHz ITU channel spacing in C band [7]. The on-chip VCL with deep-etched trenches as partially reflecting elements, is designed to provide a wavelength tuning over 20 nm at 20°C [8]. Probe light emitting out of both branches of V-cavity laser is coupled to MZI-SOAs through deep trenches. Deep-etched passive waveguides with big confinement factor are used for the delay waveguide.

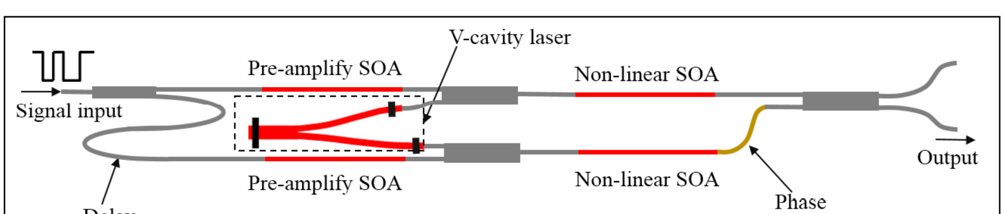

Figure 1: Schematic diagram of the monolithic wavelength converter showing the functional elements.

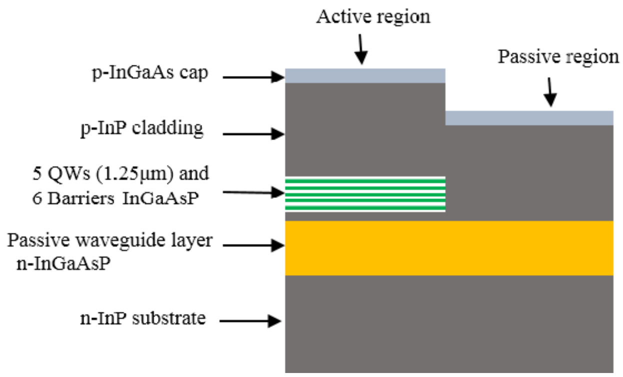

Figure 2: Cross-sectional view of the epitaxial layer structure for the offset quantum well integration platform.

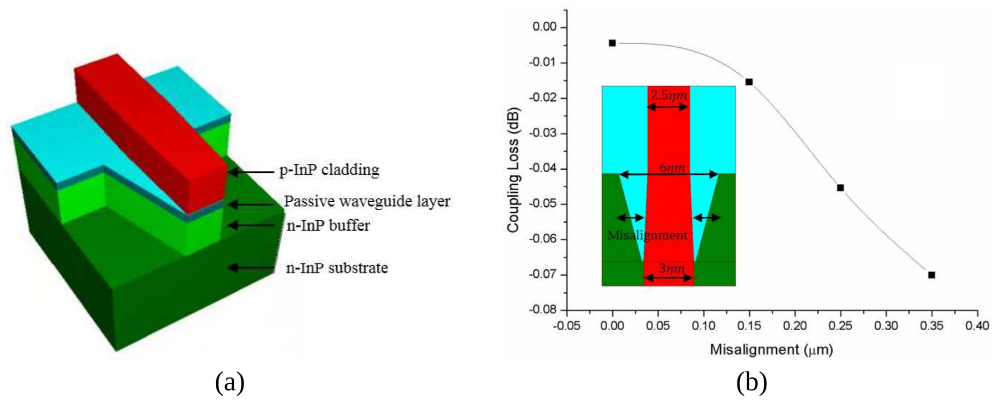

Figure 3: (a) Structure of taper between surface and deep-etch ridge waveguide. (b) Loss effect of the misalignment.

Figure 2 shows a cross-sectional view of the epitaxial layer structure for the offset quantum well integration platform. Figure 3(a) is the structure chart of the taper, which connect deep-etched passive waveguide and shallow-etched passive waveguide, can ensure coupling loss under 0.1 dB with a center misalignment tolerance of 0.5 μm as shown in Figure 3(b). The deep-etched waveguide is set 3 μm wide to reduce scattering loss of fundamental-mode on sidewall.

3. DYNAMIC SIMULATION RESULTS

DMZI structure is adopted in this design. The dynamic characteristics of the wavelength converter including optical pulse patterns, frequency chirp are investigated using the large-signal dynamic model of SOA with time-dependent transfer matrix method (TD-TMM). TD-TMM is carried out directly in time domain [10], so that it is more appropriate for dynamic characteristics simulation in a certain device than transfer matrix method (TMM) combined with multimode rate equations which is carried out in frequency domain [11].

The evolution of the slow-varying amplitude envelope $A_w(z, t)$ inside SOA's is governed by the pulse propagation equation [12, 13]

$$\frac{\partial A_w(z,t)}{\partial z} + \frac{1}{v_g}\frac{\partial A_w(z,t)}{\partial t} = -\frac{i}{2}\alpha\Gamma g_{m_w} A_w(z,t) + \frac{1}{2}(g_{m_w} - l)A_w(z,t) + \mu_w(z,t) \tag{1}$$

where w refers to different optical input signals, $A_w(z,t)$ is the pulse amplitude envelope function, α is the linewidth enhancement factor, v_g is the group velocity, Γ is the confinement factor, g_{m_w} is the material gain approximated by Equation (2) instead of Lorentzian curve in order to realise the asymmetric gain spectrum [14], l is loss constant.

$$g_{m_w}(N_i) = \frac{a_0(N_i - N_0) - a_1(\lambda_w - \lambda_p)^2 + a_2(\lambda_w - \lambda_p)^3}{1 + \varepsilon(D_1 + D_2)} \tag{2}$$

where a_0, a_1, a_2 are gain constants, λ_p is the gain peak wavelength (assumed to shift linearly with carrier density), ε is the nonlinear gain coefficient, D_1, D_2 is the photon density for signal light and probe light respectively.

The amplified spontaneous emission (ASE) noise is represented by two statistically independent Gaussian distributed random process for $\mu_w(z,t)$ [12] that satisfies Equation (3).

$$\langle \mu_w(z,t)\mu_w^*(z',t')\rangle = \beta\Gamma R_{sp}\,\delta(t-t')\delta(z-z') \times (v_g E_w A_{cross}) \tag{3}$$

where β is the spontaneous coupling factor, R_{sp} is the spontaneous emission rate, $\delta(x)$ is δ function, E_w is the photon energy, A_{cross} is the cross-sectional area of the active layer.

The relation between carrier density $N$and photon density D represented by the flowing equation:

$$\frac{\partial N}{\partial t} = \frac{I}{qV} - AN - BN^2 - CN^3 - \sum_{w=1,2} v_g \Gamma g_{m_w} D_w \tag{4}$$

where I is the injection current, q is the electronic charge, V is the volume of active area, A, B, C are nonradiative recombination coefficient, bimolecular recombination coefficient and auger recombination coefficient, respectively. The change of effective refractive index is given by $\Delta n = \Gamma\frac{dn}{dN}N$.

Figure 4 shows the schematic of the TD-TMM SOA model with reflectional facet. The SOA is divided into small sections, and the amplitudes F and R of the counter propagating optical waves update in both time and space domain using the following transfer matrix [15]:

$$\left(\frac{1}{v_g}\frac{\partial}{\partial t} \pm \frac{\partial}{\partial z}\right)\begin{bmatrix} F(z,t) \\ B(z,t) \end{bmatrix} = \begin{bmatrix} A_{11} & 0 \\ 0 & A_{22} \end{bmatrix}\begin{bmatrix} F(z,t) \\ B(z,t) \end{bmatrix} + \begin{bmatrix} S_F \\ S_B \end{bmatrix} \tag{5}$$

where A_{11}, A_{22} is self-coupling coefficients for forward and backward-going waves respectively, cross-coupling coefficients between the waves are ignored because they are much smaller comparing with self-coupling coefficients, S_F, S_B are the ASE noises coupled into the forward and backward waves.

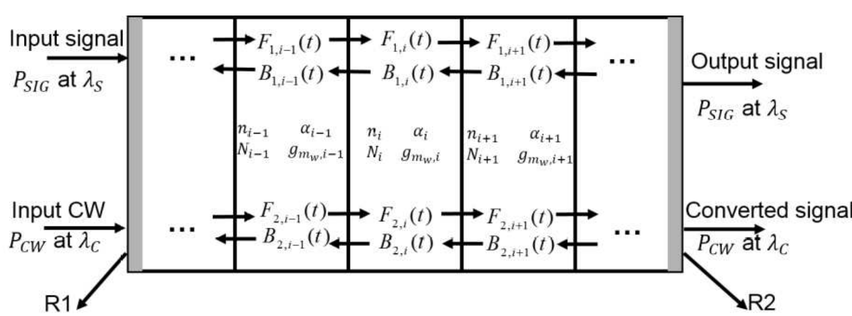

Figure 4: Schematic illustration of the TD-TMM SOA model.

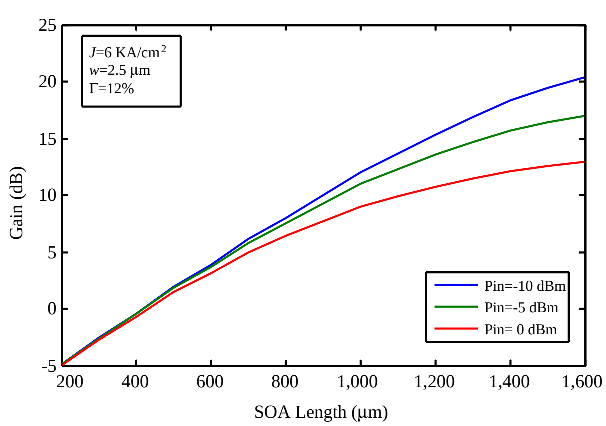

Figure 5: Simulated SOA gain versus SOA length for different input signal powers under constant current density.

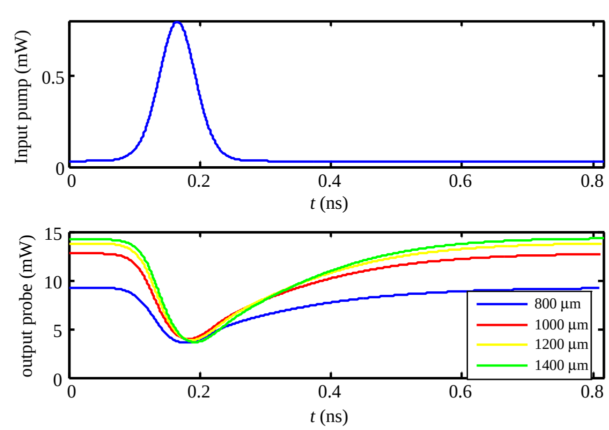

Figure 6: Simulated SOA gain recovery dynamics for different SOA length at 260 mA current injection with the input pump wavelength at 1550 nm, and the output probe at 1560 nm.

Stimulated gain versus SOA length under same current injection density for different input power levels are shown in Figure 5. Considering the coupling loss and loss of deep-etched delay waveguide, the input signal is expected under -10 dBm. Pre-amplify SOA is set 800 μm long and 2.5 μm width, with 120 mA current injection; it can offer 15 dB linear amplification.

Nolinear MZI SOAs are most important for operation of wavelength converter. When the pulse enters the upper arm, the phase of probe light changes due to carrier depletion induced by the pulse, which is a very fast process. The phase recovers slowly after the pulse has passed because of the relatively long carrier lifetime for a 10 GHz bitrate. The output of the MZI is controlled by the phase difference between the two arms. To reach a in-phase conversion, the MZI is set closed at static state, the phase shift in the first arm opens the MZI, and after the delay the other arm

Table 1: Parameters used in this simulation.

Symbol	Description	Value	Unit
Γ	Confinement factor	0.12	-
w	Waveguide width	2.5	μm
d	Thickness of active area	87.5	nm
β	Spontaneous emission coupling factor	2	-
v_g	Group velosity	8.34×10^7	m/s
A	Nonradiative recombination coefficient	1×10^8	s^{-1}
B	Bimolecular recombination coefficient	1×10^{-10}	cm^3/s
C	Active auger recombination coefficient	3.5×10^{-29}	cm^6/s
a_0	Material gain constant	2.5×10^{-20}	m^2
a_1		4.2×10^{18}	m^{-3}
a_2		5.7×10^{25}	m^{-4}
N_0	Transparent carrier density	1.4×10^{24}	m^{-3}
l	Carrier loss constant	2×10^4	m^{-1}
λ_P	Peak wavelength of material gain spectrum	1.55	μm
ε	Nonlinear gain coefficient	5×10^{-23}	m^3
α	Linewidth enhancement factor	3	
dn/dN	Index derivative wrt carrier density	-1.2×10^{-26}	m^3

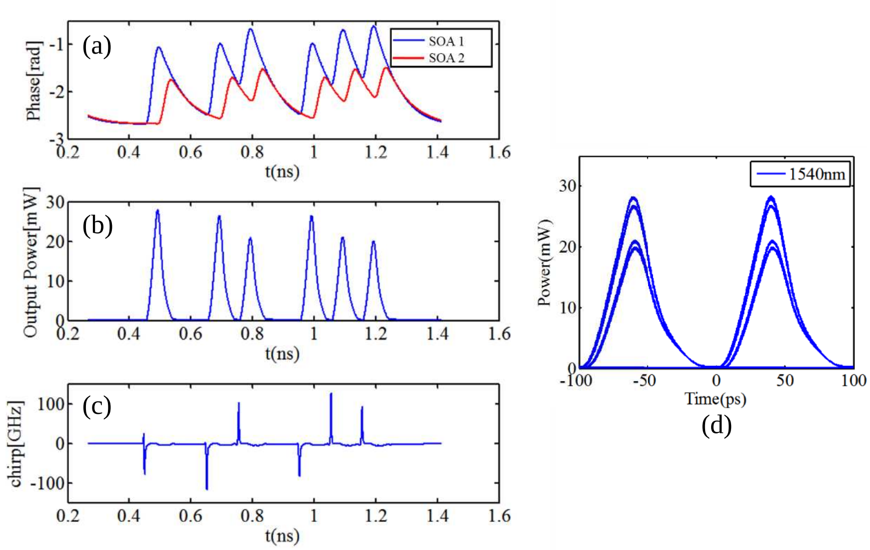

Figure 7: A simulation of (a) phase evolution, (b) output probe power, (c) frequency chirp of converted signal, (d) output eye diagram of the wavelength converter. The input pump wavelength at 1550 nm, and the output converted signal at 1540 nm.

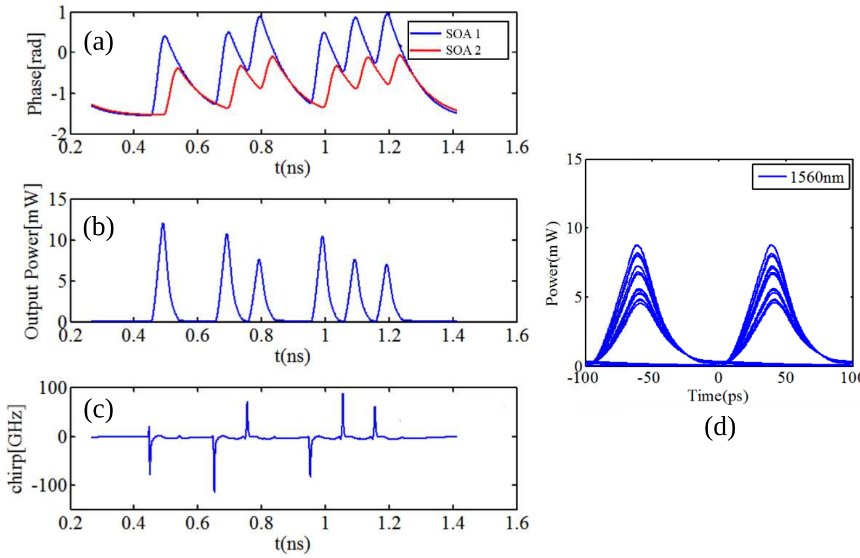

Figure 8: A simulation of (a) phase evolution, (b) output probe power, (c) frequency chirp of converted signal, (d) output eye diagram of the wavelength converter. The input pump wavelength at 1550 nm, and the output converted signal at 1560 nm.

got the same phase shift closes it. The independent control of phase change in both arms of DMZI structure makes it easier to have better performance than DISC structure [9].

With 260 mA current injection, the gain recovery phenomenon in SOA is shown in Figure 6. As it is shown, the recovery time decreases with the length of SOA increases, and become stable when longer than 1200 μm. The nonlinear-SOA is set 1200 μm long and the ridge is 2 μm wide, the recovery time is about 0.2 ns. Figure 7 and Figure 8 show the simulation results for up-conversion and down-conversion respectively. The phase change in the delayed arm is made slightly smaller to match the first one by reducing the input signal power or adjusting the current of phase section in the delayed arm. In-phase up-conversion always has lager extinction ratio and frequency chirp than down-conversion.

4. CONCLUSION

We present the design of a 10 Gb/s RZ wavelength converter based on VCL and DMZI requires very simple process technique, and give the dynamic characteristic simulation result based on SOA large-signal model with TD-TMM.

ACKNOWLEDGMENT

This work was supported by the National High-Tech R&D Program of China (grant No. 2013AA01-4401).

REFERENCES

1. Gripp, J., et al., "IRIS optical packet router," *Journal of Optical Networking*, Vol. 5, No. 8, 589–597, 2006.
2. Gripp, J., et al. "Optical switch fabrics for ultra-high-capacity IP routers," *Journal of Lightwave Technology*, Vol. 21, No. 11, 2839, 2003.
3. Stabile, R., A. Albores-Meija, and K. A. Williams, "Dynamic multi-path routing in a monolithic active-passive 16 × 16 optoelectronic switch," *Optical Fiber Communication Conference, Optical Society of America*, 2013.
4. Kamei, S., et al., "$N \times N$ cyclic-frequency router with improved performance based on arrayed-waveguide grating," *Journal of Lightwave Technology*, Vol. 27, No. 18, 4097–4104, 2009.
5. Segawa, T., et al., "A monolithic wavelength-routing switch using double-ring-resonator-coupled tunable lasers with highly reflective mirrors," *IEEE 2010 International Conference on Indium Phosphide & Related Materials (IPRM)*, 2010.

6. Mashanovitch, M., et al., "Photonic integrated circuits for optical routing and switching applications," *Optical Fiber Communication Conference, Optical Society of America*, 2011.
7. He, J.-J. and D. Liu, "Wavelength switchable semiconductor laser using half-wave V-coupled cavities," *Optics Express*, Vol. 16, No. 6, 3896–3911, 2008.
8. Zhang, S., et al., "Simple and compact V-cavity semiconductor laser with 50×100 GHz wavelength tuning," *Optics Express*, Vol. 21, No. 11, 13564–13571, 2013.
9. Ueno, Y., et al., "3.8-THz wavelength conversion of picosecond pulses using a semiconductor delayed-interference signal-wavelength converter (DISC)," *IEEE Photonics Technology Letters*, Vol. 10, No. 3, 346–348, 1998.
10. Lee, H., et al., "Theoretical study of frequency chirping and extinction ratio of wavelength-converted optical signals by XGM and XPM using SOA's," *IEEE Journal of Quantum Electronics*, Vol. 35, No. 8, 1213–1219, 1999.
11. Davis, M. G. and R. F. O'Dowd, "A transfer matrix method based large-signal dynamic model for multielectrode DFB lasers," *IEEE J. Quantum Electron.*, Vol. 30, No. 11, 2458–2466, Nov. 1994.
12. Zhang, L. M., S. F. Yu, M. C. Nowell, D. D. Marcenac, J. E. Carroll, and R. G. S. Plumb, "Dynamic analysis of radiation and side-mode suppression in a second-order DFB laser using time-domain large-signal traveling wave model," *IEEE J. Quantum Electron.*, Vol. 30, 1389–1395, 1994.
13. Agrawal, G. P. and N. A. Olsson, "Self-phase modulation and spectral broadening of optical pulses in semiconductor laser amplifiers," *IEEE J. Quantum Electron.*, Vol. 25, 2297–2306, Nov. 1989.
14. Willner, A. E. and W. Shieh, "Optimal spectral and power parameters for all optical wavelength shifting: Single stage, fanout, and cascadability," *J. Lightwave Technol.*, Vol. 13, 771–781, May 1995.
15. Li, X., *Optoelectronic Devices: Design, Modeling, and Simulation,* 184–185, Cambridge University Press, 2009.